Original Research Article: full paper

(2023), «EUREKA: Physics and Engineering»
Number 4

OPTIMIZATION OF TECHNOLOGICAL PARAMETERS WHEN POLISHING SIC MATERIALS BY MAGNETIC COMPOUND FLUID WITH THE STRAIGHT ELECTROMAGNETIC YOKE

Nguyen Minh Quang✉
Faculty of Mechanical Engineering[1]
nmqy1984@gmail.com

Nguyen Tien Tung
Faculty of Mechanical Engineering[1]

[1]*Hanoi University of Industry*
298 Cau Dien str., Bac Tu Liem dist., Hanoi, Vietnam, 100000

✉**Corresponding author**

Abstract

Crystallized silicon carbide (SiC) wafers are widely used in the field of integrated circuits as well as essential in the epitaxial growth of graphene and are one of the promising materials for applications in electronics at future high capacity. The surface quality of the required ultra-fine crystalline silicon wafer is the most essential factor in achieving graphene's desired electronic properties. Aiming to produce superfine surface quality SiC wafers, in this study, a new algorithm is developed to solve optimization problems with many nonlinear factors in ultra-precision machining by magnetic liquid mixture. The presented algorithm is a collective global search inspired by artificial intelligence based on the coordination of nonlinear systems occurring in machining processes. A new algorithm based on the optimization collaborative of multiple nonlinear systems (OCMNO) with the same flexibility and high convergence was established in optimizing surface quality when polishing the SiC wafers. To show the effectiveness of the proposed OCMNO algorithm, the benchmark functions were analyzed together with the established SiC wafers polishing optimization process. To give the best-machined surface quality, polishing experiments were set to find the optimal technological parameters based on a new algorithm and straight electromagnetic yoke polishing method. From the analysis and experimental results when polishing SiC wafers in an electromagnetic yoke field when using a magnetic compound fluid (MCF) with technological parameters according to the OCMNO algorithm for ultra-smooth surface quality with Ra = 2.306 nm. The study aims to provide an excellent reference value in optimizing surface polishing SiC wafers, semiconductor materials, and optical devices.

Keywords: OCMNO, crystallized silicon carbide wafers, magnetic compound fluid, polishing, optimization.

DOI: 10.21303/2461-4262.2023.002812

1. Introduction

With the rapid development of computer science in recent years, the research and application of AI in optimization have attracted considerable research attention and development [1–3]. However, these studies are still largely based on evolution or intelligence of creatures on earth. In general, these algorithms start with some initial solutions, and are repeated to create new solutions following certain principles and finally provide the parameters to identify the best solution during the search process [4, 5]. To overcome this issue, let's introduce a new optimization algorithm called optimise cooperation many nonlinear systems (OCMNO). In contrast to previous algorithms inspired by evolutionary phenomena in nature, the proposed algorithm is based on AI. The advantages of the proposed algorithm compared with those obtained by previous studies are expressed through the following characteristics: 1. The new operators are different from those presented by previous algorithms. 2. The convergence quality of OCMNO depends on a control parameter and is limited to a short period, thereby minimizing the familiar methods related to set control parameters. 3. The position of the elite solutions used in the revision method helps maintain the diversity of solutions, and demonstrate strength and high convergence.

In the future, with the continuous development of semiconductor technology, the semiconductor industry will be promising in the third generation of semiconductor materials. Even so, today,

the chip and semiconductor materials industry-based silicon still dominates, so it is necessary to introduce advanced technological processes for silicon semiconductor materials [6, 7]. With integrated circuit manufacturing processes, SiC wafer surface machining processes are under strict quality control. Polishing powder mixtures and methods play a very important role in SiC wafer polishing. Many studies have been conducted to obtain an ultra-smooth surface when polishing SiC wafers [8–10]. However, these processes give low surface quality, which is not suitable for the manufacturing process with the ultra-fine surface of the chips and semiconductor technology. To achieve an ultra-smooth product surface in most finishing processes, a polishing process is required to remove scratches and residual stresses above or below the surface layer. Among the existing machined surface finishing techniques, grinding or polishing by abrasive particles is commonly used. However, producing super-flat surfaces in machining processes is difficult without leaving residual stress or scratched surfaces [11–13]. In order to meet the requirements of machining ultra-precise and ultra-gloss surfaces, electromechanical polishing processes can be achieved but these processes have been shown to be less effective when applied to some materials [14, 15]. A method is being studied in recent years for surface finishing by elastic emission machining, but the material removal capacity of this method is not high [16, 17]. To overcome the disadvantages of previous methods and to produce ultra-smooth surfaces with undamaged surfaces obtained with proven efficiency and plausibility by magnetic polishing processes [18, 19]. In magnetic polishing processes, the magnetic liquid mixture under the action of a magnetic field produces a non-Newtonian liquid that exists as a hard liquid strip that serves as a flexible polishing tool [20, 21]. The shape and hardness of the magnetic fluid strip can be controlled through procedures that modulate the strength of the magnetic field thereby enhancing the performance of the magnetic polishing processes. In polishing processes with magnetic liquid mixtures, performance and operability are significantly influenced by the method and manner of magnetic field application [21–23]. When subjected to a constant magnetic field during machining processes with constant geometry and magnetic force distribution, it forms a fixed, inflexible magnetic polishing tool in finishing processes. Under the influence of a constant magnetic field, the ferromagnetic particles and abrasive particles present in the magnetic combination liquid (MCF) do not evenly disperse under the influence of the magnetic field, thereby not creating the expected polishing process. Finishing processes under the effect of an electromagnetic yoke field were established to overcome this phenomenon. The flux density can be changed within the electromagnetic yoke field and creating geometric shapes with much improved and more uniform distribution of abrasive particles under the influence of an electromagnetic yoke field.

Based on the above-mentioned characteristics, aim to create a polished model with the ultra-smooth surface of SiC wafers. In this study, the authors analyzed and developed a new mathematical model in optimization for nonlinear systems generated by machining processes. A hybrid model proposed based on the combination of the high convergence and flexibility of the proposed OCMNO algorithm with the newly developed magnetic polishing process with the electromagnetic yoke field in order to find the technological parameters for the ultra-smooth surface quality of SiC wafers. The optimized model along with the proposed electromagnetic yoke polishing process aims to further improve the surface quality, thereby providing excellent reference values for the manufacturing processes ultra-precision and the chips and semiconductor technology.

2. Materials and methods

The structure of the proposed algorithm is described based on the coordination of nonlinear objects in the group aim to find out the optimal parameters. The algorithm diagram is shown in **Fig. 1**. From here shown that just like other evolutionary optimization algorithms. The first step of the algorithm must set up the initial nonlinear objects (NLO) for the group. Based on the signal obtained from the NLOs, the NLO that acquires data larger than those collected by other NLOs in the group will act as the main NLO. The main NLO will then set up optimal situations for the group. Meanwhile, the other NLOs in the group must follow the control signal of the main NLO, which are called dependent NLO. When a dependent NLO reaches a location with a better data source than that obtained by the main NLO, the dependent NLO will become the main NLO and will act

as a guide to the group in the next part of the optimization task. Simultaneously, the previous main NLO will play the role of a dependent NLO. When implementing cooperation and optimization tasks, there is always an exchange of information between NLOs. Thus, the rank of the NLOs in the group is completely related to the location and capability to track important signals emitted from the target.

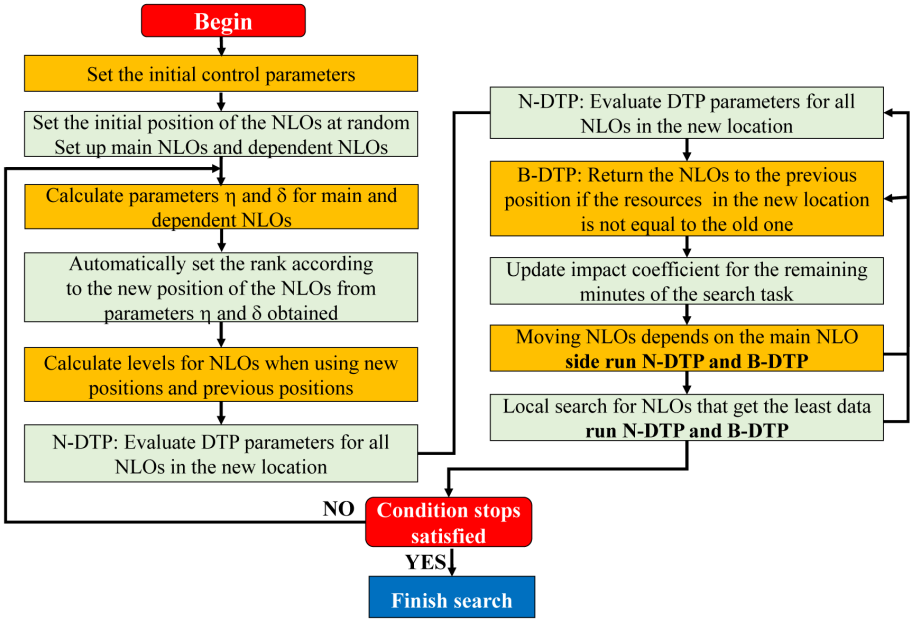

Fig. 1. Proposed OCMNO diagram

In the mission of cooperation and optimization, with the leadership of the main NLO, the following operators are formed: 1 – collection operator (concentrating NLOs depending on the position of the main NLO), 2 – exploration operator (setting search distance between main and dependent NLOs) and 3 – local search operator (establishing some dependent NLOs on the task of searching around the location of the main NLO). Compared with individuals in natural swarms, the NLOs in the group can record restrictions by previous steps. This feature allows NLOs to return to previous locations if they cannot find a convenient location during task completion.

2. 1. Set up the original NLO for the group

Optimization problems are determined by vectors of N_V decision variables to identify the position of NLOs in the search area, and the initial solution is set by an array of size $1\times N_V$. The position of the i-th NLO is determined by the following equation:

$$P_{NLO}^{i} = [x_1, x_2, ..., x_{N_v}], \tag{1}$$

where $i = 1, 2, \ldots, N$.

The parameters of x_1, x_2, ..., x_{NV} variables are determined by location. The value that displays the optimal target parameter (DTP) is determined by the equation:

$$DTP = f(P_{NLO}^{i}) = f([x_1, x_2, ..., x_{N_v}]), \tag{2}$$

where $f(P_{NLO}^{i})$ is called optimization function. Given that N is the number of NLOs in the group, the $N\times N_V$ matrix is created as an initial NLO population. The initial position of the NLOs is determined by the equation:

$$P_{NLO} = Ur(V_{MAX}, V_{MIN}, V_{side}), \tag{3}$$

where *Ur* creates a sequence of random points from a continuous uniform distribution with the lowest and highest endpoints determined by V_{MIN}, V_{MAX} and $V_{size} = 1 \times N_V$; V_{MAX} and V_{MIN} are the largest and smallest limit of decision variables, respectively.

After creating the solutions and evaluating the initial parameters, the main and dependent NLOs are determined on the basis of the DTP index.

2. 2. Collection operator

After the initial setup for the main and dependent NLOs, all dependent NLOs move to the position near the main NLO position. The collection by NLOs based on the main NLO position is conducted by random movements by the Gauss distribution function with the probability distribution density function determined as follows:

$$y = f\left[x|\eta,\sigma\right] = \frac{1}{\sigma\sqrt{2\cdot\pi}} e^{\frac{-(x-\eta)^2}{2\sigma^2}}, \tag{4}$$

where η is the average parameter, σ is the standard deviation and σ^2 is the variance. **Fig. 2** shows the probability density function for normal distribution with different parameters. During cooperation and optimization tasks, parameters η and σ are used to identify the main and dependent NLOs, respectively.

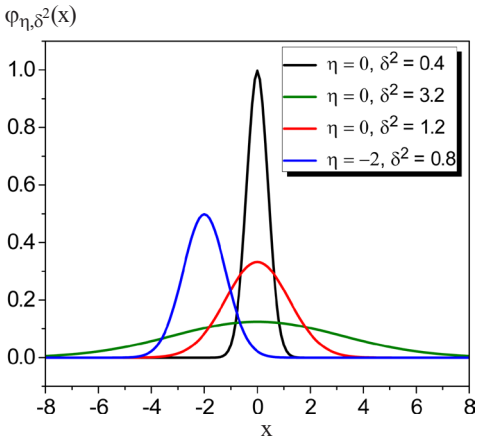

Fig. 2. Probability density function with different parameters

2. 2. 1. Calculation of parameters h and d for main and dependent NLOs

When the optimization tasks, the main NLO gathers dependent NLOs to its current location to direct them on the location with the highest resource. After the dependent NLOs gather close to the position of the main NLO, the local search process is initiated. The main NLO attempts to improve its information gathering ability to implement this search method, whilst other NLOs move to the location with the highest DTP. Considering P_1 as the first control point, the parameters h and s for the main NLO are respectively determined by the following equation:

$$\sigma_{NLO[M]} = k, \tag{5}$$

$$\eta_{NLO[M]} = \left(\frac{1 + (-1)^{E_T+1} \cdot \sigma_{NLO[M]}}{\left(\max\left[0,(-1)^{E_T+1}\right]\right) \cdot (1 - P_1) + 1} \right) \cdot P_{NLO[M]}, \tag{6}$$

where k is a random number in the range [0,1], E_T is the time taken by the search task of OCMNO and $P_{NLO[M]}$ is the location of the main NLO.

Parameters η and σ for dependent NLOs are respectively determined by the following equation:

$$\sigma_{NLO[D]} = DF^i \times \left(P_{NLO[M]} - P^i_{NLO[D]}\right) + k^2 \times P^i_{NLO[M]}(j) \Big|_{\left(P_{NLO[M]}(j) - P^i_{NLO[D]}(j)\right) < 0.05}, \tag{7}$$

$$\eta^{i}_{NLO[D]} = P_1 \times P_{NLO[M]} + (1 - P_1) \times P^{i}_{NLO[D]}, \quad (8)$$

where $i = 1, 2, \ldots, N_D$; $j = 1, 2, \ldots, N_V$ and DF^i is the parameter correction factor σ for the i-th dependent NLO.

2. 2. 2. Creation of new locations for main and dependent NLOs

The new position of the main and dependent NLOs is determined using parameters η and σ corresponding to each NLO:

$$NewP_{NLO(i)} = Gr\left(\eta_{NLO(i)}, \sigma_{NLO(i)}\right), \quad (9)$$

where the Gr function generates random points from Gauss function with parameters η and σ obtained in the previous section. The following formulas below are applied to create a relationship between the new positions obtained in the search space:

$$NewP_{NLO(i)}(j) = Max\left(V_{Min}(j), NewP_{NLO(i)}(j)\right), \quad (10)$$

$$NewP_{NLO(i)}(j) = Min\left(V_{Max}(j), NewP_{NLO(i)}(j)\right), \quad (11)$$

$$NewDTP_{NLO(i)} = f\left(NewP_{NLO(i)}\right). \quad (12)$$

2. 2. 3. Determination of DF collection parameters

When the new position of the NLOs is set, the DF parameter will be updated and modified after every minute of the search task based on changes by DTP parameters of the NLOs in the current iteration (there is reference by the previous iteration). The calculation of DF parameters is shown in **Table 1**.

$DTP^{i}_{movement}$ is determined in Step 3 before making progress assessment. Some NLOs will return to their previous position if the new locations have inappropriate DTP_{NLO} parameters.

Table 1

Calculation of DF parameters

Step	Set up and calculate parameters	Note
1	DIF = 6	Set initial parameters (modified after repetition)
2	$DF_i = DIF \times k_i$	Calculation
3	$DTP^{i}_{movement} = DTP^{i}_{NLO} - NewDTP^{i}_{NLO}$	Calculation
4	Select the i-th NLO	NLO has the largest $DTP_{movement}$
5	$DIF = \left[1 + \left\{\max\left(\overline{V_{\max}} - \overline{V_{\min}}\right)\right\} \times k\right] \times DTP_{\max}$	$DTP_{\max}$ is selected in step 4
6	DIF is obtained in the previous step $\left[0, \max\left(\overline{V_{\max}}\right)\right]$	The limit value comes from the principle 6δ
7	Switch back to step 2 to repeat the new round	–

2. 3. Exploration operator

The exploration process is where dependent NLOs are allowed to search in their surroundings when heading to the main NLO or vice versa. The location of dependent NLOs according to this policy is determined by the following equation:

$$NewP^{i}_{NLO[D]} = k \times P^{i}_{NLO[D]} + RB \times \left(P_{NLO[M]} - P^{i}_{NLO[D]}\right) \times ME, \quad (14)$$

where $RB = \pm 1$ variable is randomly selected with motion factor (ME) determined by $\max(1, |P_{NLO[M]} - P^{i}_{NLO[WD]}|)$ at the end of each iteration. The WD index refers to the dependent NLO with the lowest DTP. The ME parameter can control the convergence rate and the accuracy of the search process in different execution time intervals.

2. 4. Local search operator

In this operator, some NLOs with the lowest quality of information obtained work as worker NLOs. These NLOs are assigned to search around the location of the main NLO. However, the residence of worker NLOs at the new location only occurs when an improved position of the second-ranked NLO is realized. Otherwise, the worker NLOs will return to their previous location after the search fails. The new position of the worker NLO is determined by the following formula:

$$NewP^1_{NLO[W]} = sign\left[Rd^+\left(\left|P_{NLO[M]}\right|\right)\right]_{NLO[M]}, \tag{15}$$

$$NewP^2_{NLO[W]} = sign\left[Rd^-\left(\left|P_{NLO[M]}\right|\right)\right]_{NLO[M]}, \tag{16}$$

where $Rd^+(\bar{x})$ and $Rd^-(\bar{x})$ are the nearest integers closest to $\bar{x}$, and $sign[\Phi]_\Psi$ reflects the signs of element Ψ by element Φ:

$$NewP^3_{NLO[W]} = sign\left[RI\left(P_{NLO[M]}\right) + \left\{RF\left(P_{NLO[M]}\right)\right\}^{\frac{1}{e_1}}\right]_{NLO[M]}, \tag{17}$$

$$NewP^4_{NLO[W]} = sign\left[RI\left(P_{NLO[M]}\right) + \left\{RF\left(P_{NLO[M]}\right)\right\}^{e_2}\right]_{NLO[M]}, \tag{18}$$

where $RI(\beta)$ and $RF(\beta)$ are return functions of the integer and the dimensionless part of the β elements, respectively; the parameters e_1 and e_2 are two random integers in the interval [2, 4].

In this operator, the cross policies of the GA algorithm are applied. In particular, the new position of the fifth worker NLO is a combination of position $NewP^3_{NLO[W]}$ and $NewP^4_{NLO[W]}$ with random components R_1 and R_2, respectively (with R_1+R_2 = 100 %):

$$NewP^5_{NLO[W]} = \left[\left\{R_1\%\left(NewP^3_{NLO[W]}\right)\right\}\left\{R_2\%\left(NewP^4_{NLO[W]}\right)\right\}\right]. \tag{19}$$

This process is performed with certain variables to prevent sudden and chaotic changes in the locations where solutions are obtained.

2. 5. Convergence and optimization solution of OCMNO algorithm

The proposed algorithm is applied to non-modal functions (Fun. 1 to Fun. 9) and multimodal (Fun. 10 to Fun. 12) with small (B1), medium (B2) and large (B3) scales. These functions are described in **Table 2**.

The stop criteria of the algorithm are determined by the following formula:

$$f_{End}\left(Ro[M]\right) - Glo \le S.CA, \tag{20}$$

where $f_{End}(R_O[M])$ is the value corresponding to the solution, which is best obtained at the last iteration of the algorithm, and S.CA is the stop criterion of the algorithm. This criterion will converge with tolerances 10^{-6} and 10^{-3} corresponding to non-modal and multimodal functions, respectively. The standard deviation with the obtained results is shown as follows:

$$S.AD = \left(\frac{1}{n}\sum_{i=1}^{n}\left[x_i - \bar{x}\right]^2\right)^{\frac{1}{2}}, \tag{21}$$

where x_i is the solution result vector run by the algorithm and $\bar{x}$ is the average value of solutions determined by the following formula:

$$\bar{x} = \frac{1}{n}\sum_{i=1}^{n} x_i. \tag{22}$$

Table 2
Benchmark functions

Func.	Description	Scale			Range	Global minimum
		B1	B2	B3		
Nonmodal functions						
Fun. 1	$\sum_{i=1}^{N} X_i^2$	10	50	200	$[-100,100]$	0
Fun. 2	$\sum_{i=1}^{B}\left[100\times\left(X_i^2-x_{i+1}\right)^2+\left(1-X_i\right)^2\right]$	2	50	200	$[-10,10]$	0
Fun. 3	$1.1X\sin(2Y)+\sin(4X)\times Y$	2	–	–	$[-10,10]$	–19.8625
Fun. 4	$10N+\sum_{i=1}^{N}\left[X_i^2-10\cos(2\pi X_i)\right]$	3	50	200	$[-5.12,5.12]$	0
Fun. 5	$-20\cdot e^{\left[-0.2\sqrt{\frac{1}{30}\sum_{i=1}^{B}X_i^2}\right]}-e^{\left[-0.2\sqrt{\frac{1}{30}\sum_{i=1}^{B}\cos(2\pi X_i)}\right]}$	10	50	200	$[-30,30]$	$8.8818e^{-16}$
Fun. 6	$\sum_{i=1}^{n}\cos(X_i)\cdot\left[X_i^2+X_i\right]$	2	50	200	$[-10,10]$	–100.22365*B
Fun. 7	$\sum_{i=1}^{N}\left(\lvert X_i\rvert-10\cdot\cos\left[\sqrt{\lvert X_i\rvert}\right]\right)$	10	50	200	$[-10,10]$	–10*B
Fun. 8	$0.5+\frac{\sin^2\left[\sqrt{\left(X_1^2+X_2^2\right)}\right]-\frac{1}{2}}{0.001\left(X_1^2+X_2^2\right)+1}$	2	–	–	$[-10,10]$	0
Fun. 9	$1+\sum_{i=1}^{N}\frac{X_i^2}{4000}-\prod_{i=1}^{N}\cos\left[\frac{X_i}{\sqrt{i}}\right]$	10	50	200	$[-10,10]$	0.29289

Multimodals		Range	Global minimum	Global peak
Fun. 10	$X_1^2\times\left(\frac{X_1^4}{3}+4-2.1X_1^2\right)+4\times\left(X_2^2-1\right)\times X_2^2+X_1X_2$	$x_1\in[-1.9,1.9]$ $x_2\in[-1.1,1.1]$	–1.105	2
Fun. 11	$\left(X_1^2+X_2-11\right)^2+\left(X_1+X_2^2-7\right)^2$	$x_1\in[-10,10]$ $x_2\in[-10,10]$	0	4
Fun. 12	$\left[\sum_{i=1}^{5}i\times\cos\left\{(i-1)X_1+i\right\}\right]\times\left[\sum_{j=1}^{5}j\cdot\cos\left\{(j-1)\cdot X_2+j\right\}\right]$	$x_1\in[-10,10]$ $x_2\in[-10,10]$	–176.542	18

The parameters in **Tables 3–5** of the proposed OCMNO algorithm are compared with TLBO, GSA, PSO, and ABC after 50 times of independent implementation with the best and S.AD results obtained, which correspond to scales B1 to B3. **Table 3** shows the proposed OCMNO for the best performance. The proposed OCMNO algorithm shows that the efficiency through S.AD is lower than the mentioned algorithms. **Tables 4**, **5** show the superiority of OCMNO to the other algorithms by medium- and large-scale benchmark functions. Hence, with benchmark objective functions, in terms of solutions and quality, OCMNO shows superiority to other well-known algorithms.

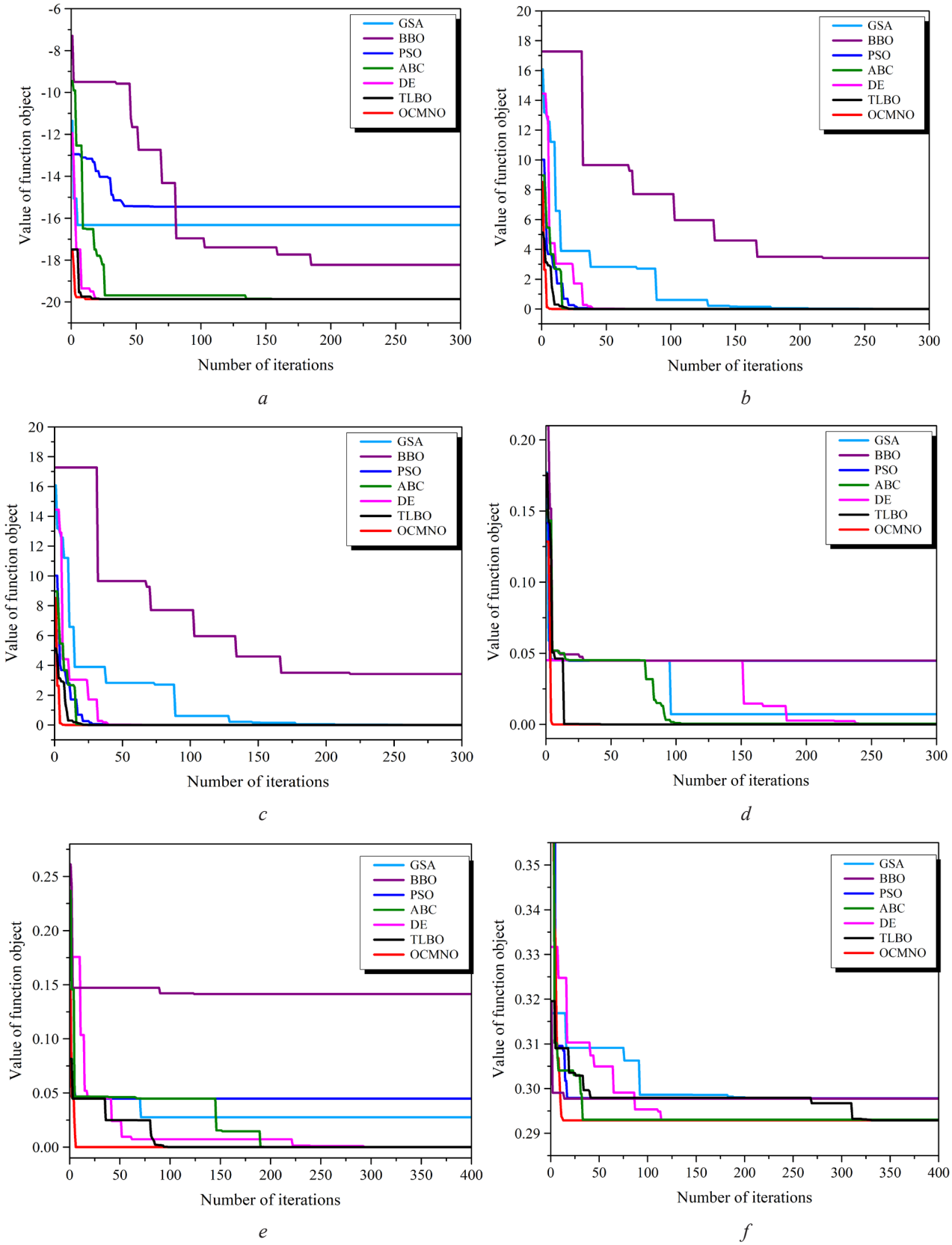

Fig. 3. Convergence capability with different optimization algorithms: *a* – Fun. 3; *b* – Fun. 5; *c* – Fun. 6; *d* – Fun. 7; *e* – Fun. 8; *f* – Fun. 9

Table 3
Small scale (B1) with non-modal functions benchmark functions

No.	Parameter	Algorithms				
		TLBO	GSA	PSO	ABC	OCMNO
Fun. 1	Best	$3.25{\cdot}e^{-6}$	5.8265	$4.15{\cdot}e^{-14}$	0.0369	0
	S.AD	$1.81{\cdot}e^{-4}$	4.0362	$2.69{\cdot}e^{-11}$	0.3498	0
Fun. 2	Best	$6.82{\cdot}e^{-5}$	0.0085	$3.14{\cdot}e^{-16}$	$5.62{\cdot}e^{-7}$	0
	S.AD	0.0325	0.2915	$1.04{\cdot}e^{-8}$	0.0036	0
Fun. 3	Best	−19.8625	−19.7734	−19.8625	−19.8624	−19.8625
	S.AD	$5.72{\cdot}e^{-04}$	0.5189	1.9550	$4.46{\cdot}e^{-10}$	$1.68{\cdot}e^{-06}$
Fun. 4	Best	0	1.0313	0	$1.98{\cdot}e^{-6}$	0
	S.AD	$8.79{\cdot}e^{-13}$	1.5538	1.3154	0.4332	0
Fun. 5	Best	0.0028	4.8954	$5.33{\cdot}e^{-8}$	0.1133	$8.88{\cdot}e^{-16}$
	S.AD	0.1333	0.5293	0.4348	0.2695	0
Fun. 6	Best	−200.4473	−200.4396	−200.4476	−200.447	−200.4474
	S.AD	$1.56{\cdot}e^{-12}$	1.3388	42.3978	2.6665	$1.07{\cdot}e^{-04}$
Fun. 7	Best	−80.2418	−45.7485	−76.7760	−76.2008	−100
	S.AD	2.8902	3.5163	4.2107	3.4835	0
Fun. 8	Best	$1.23{\cdot}e^{-4}$	$3.61{\cdot}e^{-5}$	0	0	0
	S.AD	0.0105	0.0065	0.0218	$6.66{\cdot}e^{-9}$	0
Fun. 9	Best	$6.35{\cdot}e^{-5}$	0.3206	0	$4.38{\cdot}e^{-4}$	0
	S.AD	0.0165	0.1002	0.0314	0.1068	0

Table 4
Medium scale (B2) with non-modal functions benchmark functions

No.	Parameter	Algorithms				
		TLBO	GSA	PSO	ABC	OCMNO
Fun. 1	Best	0.0771	201.0651	85.7738	20.9615	0
	S.AD	1.1830	65.5293	95.5022	238.9055	0
Fun. 2	Best	49.0557	$7.15{\cdot}e^{4}$	158.6456	432.4415	48.5065
	S.AD	0.8573	$4.90{\cdot}e^{4}$	152.5239	$1.76{\cdot}e^{4}$	0.1061
Fun. 3	Best	24.8026	478.2613	65.4385	0	0
	S.AD	42.8524	17.3122	22.4825	85.3015	0
Fun. 4	Best	0.0619	8.2536	2.7345	5.9036	$8.88{\cdot}e^{-16}$
	S.AD	0.0934	0.3456	1.0962	2.1066	0
Fun. 5	Best	−4694.7	−1182.8	−2882.1	−4235.6	−4813.5
	S.AD	81.2471	134.3851	285.16	183.5909	62.75
Fun. 6	Best	−299.1726	−115.5256	−350.1128	−316.7345	−500
	S.AD	11.4561	11.6326	8.5081	15.6361	0
Fun. 7	Best	$3.25{\cdot}e^{-5}$	0.9831	0.0032	0.0286	0
	S.AD	$2.35{\cdot}e^{-4}$	0.0126	0.0216	0.1193	0
Fun. 8	Best	0.0771	201.0651	85.7738	20.9615	0
	S.AD	1.1830	65.5293	95.5022	238.9055	0
Fun. 9	Best	49.0557	$7.15{\cdot}e^{4}$	158.6456	432.4415	48.5065
	S.AD	0.8573	$4.90{\cdot}e^{4}$	152.5239	$1.76{\cdot}e^{4}$	0.1061

Table 5
Large scale (B3) with non-modal functions benchmark functions

No.	Parameter	Algorithms				
		TLBO	GSA	PSO	ABC	OCMNO
Fun. 1	Best	0.6035	$4.89 \cdot e^{3}$	10114	$1.36 \cdot e^{5}$	0
	S.AD	1.4665	$1.97 \cdot e^{3}$	2378.4	$2.43 \cdot e^{4}$	0
Fun. 2	Best	200.1315	$4.24 \cdot e^{5}$	41084	$3.48 \cdot e^{6}$	198.5726
	S.AD	2.8213	$1.39 \cdot e^{5}$	18630	$1.55 \cdot e^{6}$	0.0602
Fun. 3	Best	18.5444	$1.89 \cdot e^{3}$	777.5746	$1.47 \cdot e^{3}$	0
	S.AD	29.4734	63.1346	65.0408	96.1149	0
Fun. 4	Best	0.0858	10.2015	9.7025	18.4186	$8.88 \cdot e^{-16}$
	S.AD	0.0642	0.3714	0.7685	0.2469	0
Fun. 5	Best	−17853	−3206.5	−7706.1	−11734	−18014
	S.AD	226.7121	273.3312	1638.1	505.3369	407.7908
Fun. 6	Best	−636.733	−489.083	−789.643	−957.402	−2000
	S.AD	68.1022	51.9533	50.7421	133.2738	0
Fun. 7	Best	$4.05 \cdot e^{-5}$	1.1069	0.5448	1.3414	0
	S.AD	$1.28 \cdot e^{-4}$	0.0168	0.0936	0.523	0
Fun. 8	Best	0.6035	$4.89 \cdot e^{3}$	10114	$1.36 \cdot e^{5}$	0
	S.AD	1.4665	$1.97 \cdot e^{3}$	2378.4	$2.43 \cdot e^{4}$	0
Fun. 9	Best	200.1315	$4.24 \cdot e^{5}$	41084	$3.48 \cdot e^{6}$	198.5726
	S.AD	2.8213	$1.39 \cdot e^{5}$	18630	$1.55 \cdot e^{6}$	0.0602

When applying algorithms for multimodal functions (Fun. 10, Fun. 12) based on time, the average value (mean value of all algorithm runs) and the optimal average value (average number of peaks found above 50 times with S.CA = 1000) are shown in **Table 6**. Based on the results, the possibility of multimodal functions is not as high as that of non-modal functions. The complexity of the benchmark functions from Fun.10 to Fun. 12 increases, thereby realizing the reduction of the quality of solutions. This process is expressed via analysis. The average optimization value (AO) corresponding to the Fun. 10 function is 2 (100 % success rate). However, the AO value with Fun. 12 function achieved by OCMNO is 16.98 (94.3 % success rate). The results show that the quality obtained by OCMNO is superior to the algorithms mentioned in most cases. Therefore, OCMNO has high applicability on target identification with nonlinear systems and various optimization problems.

Table 6
Optimal solution with multimodal functions

Func.	Characteristics	Optimization algorithms				
		GSA	PSO	ABC	TLBO	OCMNO
Fun. 10	Time reached	33	46	48	49	8.03
	Average value	−0.9784	−1.0175	−1.02803	−1.03151	−1.03162
	OA value	1.69	1.89	1.93	1.98	2
Fun. 11	Time reached	3	37	40	43	47
	Average value	$4.5215 \cdot e^{-3}$	$5.7579 \cdot e^{-6}$	$3.2535 \cdot e^{-6}$	$4.2859 \cdot e^{-7}$	$4.6293 \cdot e^{-8}$
	OA value	2.67	3.49	3.55	3.63	3.79
Fun. 12	Time reached	18	29	32	34	40
	Average value	−152.2436	−169.5681	−170.8427	−173.8542	−175.7125
	OA value	8.01	11.79	12.67	13.39	16.98

3. Results and discussion

Fig. 4 describes the polishing principle of SiC material using an MCF in an electromagnetic yoke field. The MCF composite is placed above the electromagnet and a distance of H from the magnet using an aluminium carrier disc. The principle of creating an electromagnetic yoke field by an electromagnet placed with a distance *R* below the rotating disk. Straight clearance increased the contact area between the MCF and the workpiece. Axis 2, during rotation, will transmit n_2 rotation to the MCF. Under the rotating action of the MCF, the polishing force is acting on the workpiece, and the MCF polishing is established when the workpiece is placed under the MCF carrier plate at a distance of *K*.

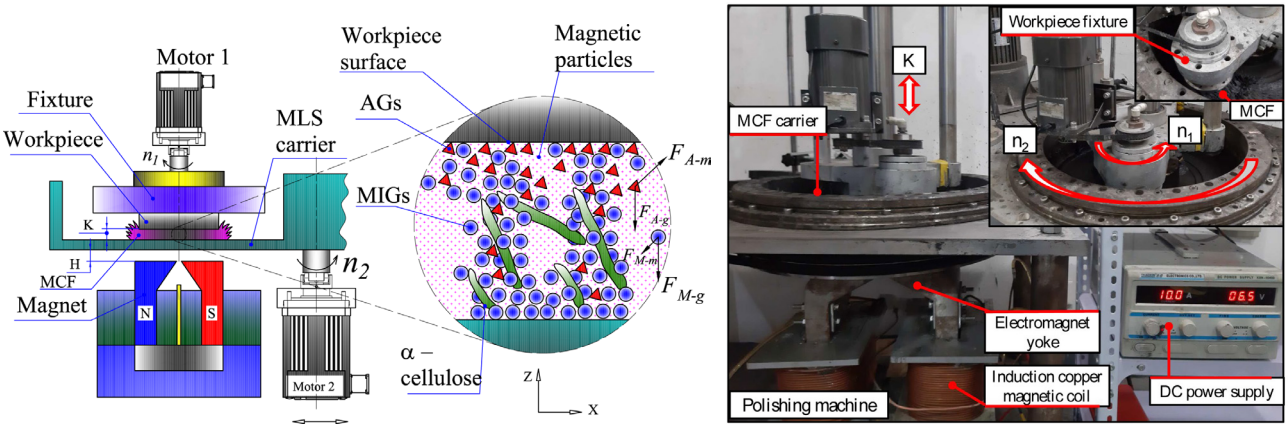

a *b*

Fig. 4. Polishing SiC material in electromagnetic yoke field:
a – schematic diagram; *b* – experimental setup

When an electromagnetic yoke field is applied, the shape and geometrical position of the assemblies will always form a straight MCF band due to the magnetic attraction. In the MCF polishing setup, an electromagnetic yoke field is generated based on an electromagnet made with electromagnet with adjustable magnetic field strength. The composition of the MCF is shown in **Table 7**.

Table 7
MCF components set up

Description	Parameters	Relative permeability	Material
Electromagnets current	5, 7, 9, 11 A	1.09977	Ferromagnetic
Percentage of components in MCF			
CIP (Carbonyl iron particles)	1 µm	44 %	Ferromagnetic
	3 µm	44 %	
	5 µm	44 %	
	8 µm	44 %	
AP (Abrasive particles)	5 µm	8 %	Diamond
	3 µm	8 %	
	1 µm	8 %	
	0.5 µm	8 %	

Under the effect of the magnetic field when the MCF polishing processes are established, micrometre-sized magnetic particles are formed in the magnetic induction directions. Under the effect of magnetic particles combined with cellulose fibres present in the MCF during operation, the magnetic abrasive particles will follow the action of the magnetic induction line under the effect of the magnetic field. When the n1 motor rotates, it will transmit motion to the

aluminium disc, through which the MCF polishing mixture will transmit rotation to the abrasive particles thereby creating a cutting action with a very small depth of cut by micro-sized abrasive particles. The experimental parameters to find the optimal factor for the best surface quality is described in **Table 8**.

Table 8
Technological parameters when polishing SiC material under electromagnetic yoke field

Level	Working distance	AP diameter	CIP diameter	Current
1	0.8 mm	5 µm	1 µm	5 A
2	1 mm	3 µm	3 µm	7 A
3	1.5 mm	1 µm	5 µm	9 A
4	3 mm	0.5 µm	8 µm	11 A

The SiC workpieces after polishing were averaged for surface roughness at three different locations by the Zygo 7100 roughness measuring device. Polishing parameters conducted according to Taguchi L16 experimental analysis after 90 minutes of polishing are described in **Table 9** and **Fig. 6**.

Table 9
Experimental results when MCF polishing with electromagnetic yoke field for SiC material

No.	Polishing mode				Roughness mean Ram (nm)	S/N ratio
	Working distance	CIP diameter	AP diameter	Current		
1	0.8 mm	1 µm	0.5 µm	5 A	10,093	–20,08
2	0.8 mm	3 µm	1 µm	7 A	8,427	–18,51
3	0.8 mm	5 µm	3 µm	9 A	8,557	–18,65
4	0.8 mm	8 µm	5 µm	11 A	11,081	–20,89
5	1 mm	1 µm	3 µm	9 A	20,716	–26,33
6	1 mm	3 µm	5 µm	11 A	7,376	–17,36
7	1 mm	5 µm	0.5 µm	5 A	8,445	–18,53
8	1 mm	8 µm	1 µm	7 A	16,119	–24,15
9	1.5 mm	1 µm	1 µm	11 A	18,643	–25,41
10	1.5 mm	3 µm	0.5 µm	9 A	11,063	–20,88
11	1.5 mm	5 µm	5 µm	7 A	7,460	–17,45
12	1.5 mm	8 µm	3 µm	5 A	12,149	–21,69
13	3 mm	1 µm	1 µm	7 A	22,784	–27,15
14	3 mm	3 µm	0.5 µm	5 A	10,732	–20,61
15	3 mm	5 µm	3 µm	11 A	9,951	–19,96
16	3 mm	8 µm	5 µm	9 A	10,221	–20,19

The results in **Fig. 5** show the ANOVA analysis of surface quality with experimental parameters described in **Table 9** for the S/N ratio corresponds to the working distance, CIP diameter, AP diameter, and current are (–16.71), (–12.84), (–16.12) and (–16.90) levels for 1311 levels (corresponding workpiece distance 0.8 mm; AP diameter 0.5 mm; CIP diameter 5 mm; Current 6 A).

The surface quality results obtained before and after polishing as described in **Fig. 6** show that the surface has been significantly improved by the proposed electromagnetic yoke field polishing method. With the experimental results obtained in **Table 9** and **Fig. 6**, when applying the proposed optimization algorithm OCMNO and ANOVA analysis to further improve the surface quality, the technological parameters are obtained when optimizing for the polishing process of SiC materials by electromagnetic yoke field as described in **Table 10**.

Factor	Average S/N by levels			
	Working distance	CIP diameter	AP diameter	Current
1	-19,53	-24,74	-18,09	-20,23
2	-20,78	-19,34	-21,62	-21,14
3	-22,24	-17,97	-22,20	-21,68
4	-21,98	-21,73	-21,86	-20,90
Max	-19,53	-17,97	-18,09	-20,23
Opt. plan	1311 (Working distance 0.8 mm; AP sizes 0.5 µm; Current 5 A; CIP sizes 5 µm)			

a

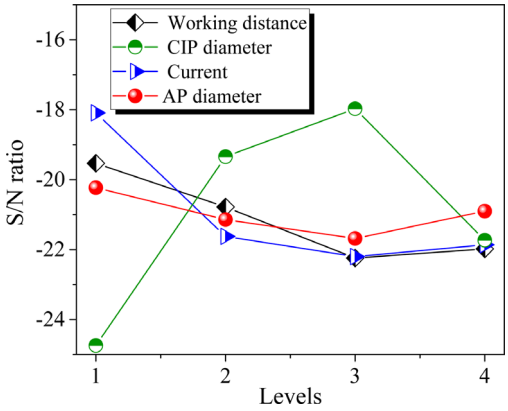

b

Fig. 5. Results of experimental analysis of ANOVA for polishing material SiC

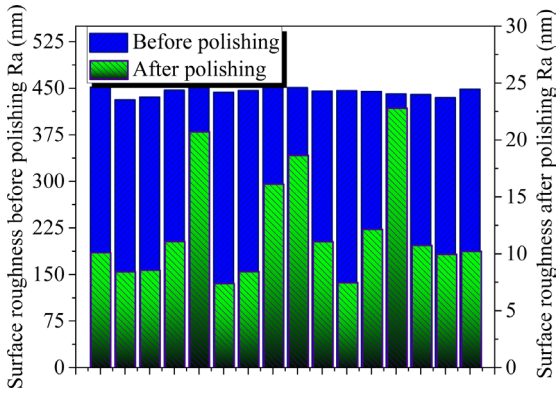

Fig. 6. Surface quality before and after polishing MCF with an electromagnetic yoke for SiC material

Table 10
Optimal polishing parameters according to ANOVA and OCMNO analysis

Optimize polishing mode	Working distance	CIP diameter	AP diameter	Current
ANOVA	0.8 mm	5 µm	0.5 µm	5 A
OCMNO	0.85 mm	3.5 µm	1 µm	5.8 A

From the optimal results through ANOVA analysis and the proposed OCMNO algorithm, experimental verification processes are established.

The verification experimental results depicted in **Fig. 7** after 90 minutes of polishing show that with the experimental analysis according to ANOVA for surface quality (Ra = 6.135 nm), the results show that the surface quality is improved better than the experimental according to Taguchi L16 as given in **Table 5**. However, the surface under optimal conditions with experimental analysis of ANOVA still appears a few very small scratches. The ultra-smooth surface with no scratches on the surface obtained experimentally according to the polishing parameters proposed by the OCMNO optimization algorithm.

Experimenting according to the technological mode proposed by OCMNO gives the superfine surface quality with Ra = 2.306 nm, along with that, the surface quality is improved by 62.41 % compared to the optimization according to the experimental analysis ANOVA.

The obtained results show that the optimization algorithm and the proposed polishing model are capable of creating an ultra-smooth surface for SiC material without any scratches.

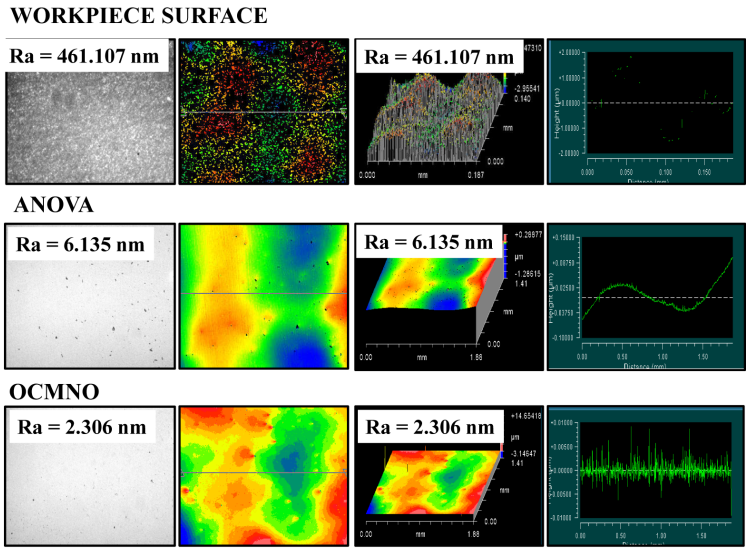

Fig. 7. Surface morphology when polishing verified under optimal cutting modes

In this work, the optimization model of the polishing process with MCF slurry under the effect of a straight electromagnetic yoke field has been studied and given the optimal set of technological parameters. The ultra-fine surface quality obtained from the proposed optimization model shows the high industrial applicability of the proposed model. However, in the present study, the authors have not investigated the working life of MCF slurry. In addition, the effect of the magnetic field on the structure of MCF slurry and the material removed rate has not been analyzed. Future work should be done to clarify the service life of the MCF slurry. Along with that, it is necessary to systematically study the effects of magnetic forces on abrasives and magnetic particles in MCF polishing processes. Based on the characteristic removal function, MCF polishing is capable of finishing free-form surfaces by designing a certain polishing path.

4. Conclusions

A new OCMNO algorithm is proposed based on NLO. The analytical procedures include benchmark functions to evaluate the performance of the presented optimization algorithms in terms of solution, quality and speed of convergence. The analysis results show that the quality obtained by the proposed OCMNO algorithm is superior to the mentioned algorithms in most cases. Therefore, the proposed OCMNO algorithm exhibits high applicability for nonlinear systems and other optimization problems.

Experimental results of polishing with a straight electromagnetic yoke field for SiC material capable of creating an ultra-smooth surface with surface roughness obtained in nanometer form when following the technological parameters by the algorithm OCMNO suggested. The verification experiments obtained a superfine surface with Ra = 2.306 nm according to the working distance, AP diameter, CIP diameter, and current with polishing parameters 0.85 mm, 1 μm, 3.5 μm and 5.8 A, respectively. The optimized surface quality has been increased by 62.41 % when choosing technological parameters according to the OCMNO optimization algorithm compared to the results of the experimental optimization analysis. The proposed polishing and optimization model is capable of obtaining a superfine surface in nanometer form for SiC material from inexpensive polishing materials such as commercial CIP, and AP particles. Thereby creating great potential in ultra-precision machining of SiC wafers in particular, as well as semiconductor materials and optical lenses.

Conflict of interest

The authors declare that there is no conflict of interest in relation to this paper, as well as the published research results, including the financial aspects of conducting the research, obtaining and using its results, as well as any non-financial personal relationships.

Financing

The study was performed without financial support.

Data availability

Data will be made available on reasonable request.

Acknowledgements

The work described in this paper was supported by Ha Noi University of Industry (HaUI) for a scientific project.

References

[1] Ramírez-Duque, A. A., Frizera-Neto, A., Bastos, T. F. (2019). Robot-Assisted Autism Spectrum Disorder Diagnostic Based on Artificial Reasoning. Journal of Intelligent & Robotic Systems, 96 (2), 267–281. doi: https://doi.org/10.1007/s10846-018-00975-y

[2] Al-Mufti, F., Dodson, V., Lee, J., Wajswol, E., Gandhi, C., Scurlock, C. et al. (2019). Artificial intelligence in neurocritical care. Journal of the Neurological Sciences, 404, 1–4. doi: https://doi.org/10.1016/j.jns.2019.06.024

[3] Jha, K., Doshi, A., Patel, P., Shah, M. (2019). A comprehensive review on automation in agriculture using artificial intelligence. Artificial Intelligence in Agriculture, 2, 1–12. doi: https://doi.org/10.1016/j.aiia.2019.05.004

[4] Khare, A., Rangnekar, S. (2013). A review of particle swarm optimization and its applications in Solar Photovoltaic system. Applied Soft Computing, 13 (5), 2997–3006. doi: https://doi.org/10.1016/j.asoc.2012.11.033

[5] Maier, H. R., Razavi, S., Kapelan, Z., Matott, L. S., Kasprzyk, J., Tolson, B. A. (2019). Introductory overview: Optimization using evolutionary algorithms and other metaheuristics. Environmental Modelling & Software, 114, 195–213. doi: https://doi.org/10.1016/j.envsoft.2018.11.018

[6] Kim, J. G., Kim, Y. H., Choi, D. J. (2014). Improved electrical properties of SiC wafer with defects covered by free standing graphene. Diamond and Related Materials, 43, 55–59. doi: https://doi.org/10.1016/j.diamond.2014.01.010

[7] Srivastava, M., Pandey, P. M., Kuldeep, Basheed, G. A., Pant, R. P. (2021). Synthesis and characterization of the rheological behavior of MR fluid for polishing silicon wafer using double-disc chemical-assisted magneto-rheological finishing process. Journal of Magnetism and Magnetic Materials, 534, 168044. doi: https://doi.org/10.1016/j.jmmm.2021.168044

[8] Mosavat, M., Rahimi, A. (2019). Numerical-experimental study on polishing of silicon wafer using magnetic abrasive finishing process. Wear, 424-425, 143–150. doi: https://doi.org/10.1016/j.wear.2019.02.007

[9] Srivastava, M., Singh, J., Mishra, D. K., Singh, R. P. (2022). Review on the various strategies adopted for the polishing of silicon wafer – A chemical perspective. Materials Today: Proceedings, 63, 62–68. doi: https://doi.org/10.1016/j.matpr.2022.02.300

[10] Huo, F., Guo, D., Kang, R., Feng, G. (2012). Nanogrinding of SiC wafers with high flatness and low subsurface damage. Transactions of Nonferrous Metals Society of China, 22 (12), 3027–3033. doi: https://doi.org/10.1016/s1003-6326(11)61566-5

[11] Kang, R., Zhang, Y., Gao, S., Huang, J., Zhu, X. (2022). High surface integrity fabrication of silicon wafers using a newly developed nonwoven structured grind-polishing wheel. Journal of Manufacturing Processes, 77, 229–239. doi: https://doi.org/10.1016/j.jmapro.2022.03.021

[12] Zhu, W.-L., Beaucamp, A. (2020). Compliant grinding and polishing: A review. International Journal of Machine Tools and Manufacture, 158, 103634. doi: https://doi.org/10.1016/j.ijmachtools.2020.103634

[13] Duc, L. A., Hieu, P. M., Quang, N. M. (2022). Study chemical reaction of –Si–OH surface layer by solid and ionic form to surface quality when polishing with chemical-mechanical slurry. Journal of King Saud University – Engineering Sciences. doi: https://doi.org/10.1016/j.jksues.2022.08.002

[14] Bai, J., Xu, Z., Qian, L. (2022). Precision-improving manufacturing produces ordered ultra-fine grained surface layer of tungsten heavy alloy through ultrasonic elliptical vibration cutting. Materials & Design, 220, 110859. doi: https://doi.org/10.1016/j.matdes.2022.110859

[15] Lu, A., Shang, Z., Luo, X., Jin, T., Luo, H. (2020). Rapid fabrication of ultra-smooth Y-TZP bioceramic surfaces by dual-axis wheel polishing: process development and tribological characterization. Journal of Manufacturing Processes, 55, 276–287. doi: https://doi.org/10.1016/j.jmapro.2020.04.055

[16] Hirata, T., Takei, Y., Mimura, H. (2014). Machining Property in Smoothing of Steeply Curved Surfaces by Elastic Emission Machining. Procedia CIRP, 13, 198–202. doi: https://doi.org/10.1016/j.procir.2014.04.034

[17] Kanaoka, M., Takino, H., Nomura, K., Mori, Y., Mimura, H., Yamauchi, K. (2007). Removal properties of low-thermal-expansion materials with rotating-sphere elastic emission machining. Science and Technology of Advanced Materials, 8 (3), 170–172. doi: https://doi.org/10.1016/j.stam.2006.12.003

[18] Duy, N. T., Tien, D. H., Thoa, P. T. T. (2022). A new environment-friendly magnetorheological finishing and fuzzy grey relation analysis in Ti-6Al-4V alloy polishing. Manufacturing Review, 9, 17. doi: https://doi.org/10.1051/mfreview/2022013

[19] Xiao, C., Hsia, F.-C., Sutton-Cook, A., Weber, B., Franklin, S. (2022). Polishing of polycrystalline diamond using synergies between chemical and mechanical inputs: A review of mechanisms and processes. Carbon, 196, 29–48. doi: https://doi.org/10.1016/j.carbon.2022.04.028

[20] Wang, C., Loh, Y. M., Cheung, C. F., Wang, S., Ho, L. T., Li, Z. (2022). Shape-adaptive magnetic field-assisted batch polishing of three-dimensional surfaces. Precision Engineering, 76, 261–283. doi: https://doi.org/10.1016/j.precisioneng.2022.04.003

[21] Xia, Z., Fang, F., Ahearne, E., Tao, M. (2020). Advances in polishing of optical freeform surfaces: A review. Journal of Materials Processing Technology, 286, 116828. doi: https://doi.org/10.1016/j.jmatprotec.2020.116828

[22] Tien, D. H., Duy, T. N., Thoa, P. T. T. (2022). Applying GPR-FGRA hybrid algorithm for prediction and optimization of eco-friendly magnetorheological finishing Ti–6Al–4V alloy. International Journal on Interactive Design and Manufacturing (IJIDeM), 17 (2), 729–745. doi: https://doi.org/10.1007/s12008-022-00995-x

[23] Zhou, D., Huang, X., Ming, Y., Li, X., Li, H., Li, W. (2021). Material removal characteristics of magnetic-field enhanced shear thickening polishing technology. Journal of Materials Research and Technology, 15, 2697–2710. doi: https://doi.org/10.1016/j.jmrt.2021.09.092

Received date 10.03.2023
Accepted date 13.06.2023
Published date 27.07.2023

How to cite: *Quang, N. M., Tung, N. T. (2023). Optimization of technological parameters when polishing sic materials by magnetic compound fluid with the straight electromagnetic yoke. EUREKA: Physics and Engineering, 4, 104–119. doi: https://doi.org/10.21303/2461-4262.2023.002812*